AGU PUBLICATIONS

JGR

Journal of Geophysical Research: Space Physics

RESEARCH ARTICLE
10.1002/2014JA019807

Key Points:
- First work on solar cycle, seasonal, and diurnal variations of SAID
- SAID is the product of the coupling magnetosphere-ionosphere system

Correspondence to:
X.-X. Zhang,
xxzhang@cma.gov.cn

Citation:
He, F., X.-X. Zhang, and B. Chen (2014), Solar cycle, seasonal, and diurnal variations of subauroral ion drifts: Statistical results, *J. Geophys. Res. Space Physics*, *119*, 5076–5086, doi:10.1002/2014JA019807.

Received 21 JAN 2014
Accepted 29 MAY 2014
Accepted article online 9 JUN 2014
Published online 20 JUN 2014

Solar cycle, seasonal, and diurnal variations of subauroral ion drifts: Statistical results

Fei He[1], Xiao-Xin Zhang[2], and Bo Chen[1]

[1]Changchun Institute of Optics, Fine Mechanics and Physics, Chinese Academy of Sciences, Changchun, China, [2]National Center for Space Weather, China Meteorological Administration, Beijing, China

Abstract The solar cycle, seasonal, and diurnal variations of the subauroral ion drifts (SAIDs) are investigated for the first time to use such a large database of 18,226 SAID events observed by the DMSP satellites during 1987–2012. Statistical results show that SAIDs occur mostly at 60.1° invariant latitude and 2230 magnetic local time with a typical half width of 0.57°, move equatorward during high solar activities with large widths, and have two occurrence peaks in spring and fall equinoxes and two valleys in summer and winter solstices. The seasonal variation of SAID latitude has two valleys in spring and fall, and SAID width has a valley distribution with a minimum in summer. SAIDs exhibit a clear day-to-night difference in latitude. The diurnal variation of SAID width has a morning valley and an afternoon peak. The generation mechanism of SAID associated with the electron precipitation and the downward field-aligned current is also supported in this study.

1. Introduction

The subauroral ion drifts (SAIDs) are geomagnetic activity-related rapid westward ion drifts (WID) or strong poleward electric field (PEF) on the nightside equatorward of the auroral ionosphere during magnetospheric substorms (especially during their recovery phases). *Galperin et al*. [1973] first reported the PEF phenomena and called them polarization jets (PJ). They were subsequently termed as SAID by *Spiro et al*. [1979]. They have been widely observed by many satellites, being the most significant convection feature of the coupled magnetosphere-ionosphere (MI) system during substorms [*Maynard et al*., 1980; *Anderson et al*., 1991, 1993, 2001; *Foster et al*., 1994; *Karlsson et al*., 1998; *Puhl-Quinn et al*., 2007, and references therein]. In these referenced works, SAID/PJ just refers to narrow and transient region of subauroral electric field and plasma flow. Then, *Yeh et al*. [1991] reported broader regions of sunward plasma drift, equatorward of and separated from the evening auroral convection cell. *Foster and Burke* [2002] suggested an inclusive name, subauroral polarization streams (SAPS), to encompass the SAID/PJ and the broader regions reported by *Yeh et al*. [1991]. From then on, characteristics of SAPS and their effects are investigated by many works through data analysis [*Foster and Vo*, 2002; *Foster et al*., 2004; *Anderson*, 2004; *Oksavik et al*., 2006; *Huang and Foster*, 2007; *Wang et al*., 2008, 2012, and references therein] and model simulations [*Goldstein et al*., 2005; *Lyatsky et al*., 2006; *Pintér et al*., 2006; *Zheng et al*., 2008, etc.].

During substorms and especially during their recovery phases, SAID often appears as the intense convection zone characterized by a latitudinally narrow (~1°–2°) and longitudinally elongated (~1600–0300 magnetic local time (MLT)) region in the equatorward subauroral ionosphere with a WID peak greater than 1000 m/s (corresponding to a poleward electric field of ~30 mV/m). SAIDs have significant effects on the ionosphere and the plasmasphere, such as ionospheric composition changes [*Anderson et al*., 1991], very deep *F* region density troughs [*Spiro et al*., 1978], very large field-aligned vertical flows [*Rich et al*., 1980; *Anderson et al*., 1991], plasmaspheric troughs inside or outside the plasmapause [*Ober et al*., 1997; *He et al*., 2012], and the plasmaspheric short circuit of substorm injections [*Mishin and Puhl-Quinn*, 2007].

There are many case studies and statistical investigations concerning the characteristics of SAID distributions and the relationships between SAID features and geomagnetic activities. SAIDs occur mostly at 60° invariant latitude (ILAT) and 2200 MLT with majority between 55°–65° ILAT and 2100–2300 MLT [*Karlsson et al*., 1998; *Figueiredo et al*., 2004; *He et al*., 2012] with a lifetime of less than ~3 h and a latitudinal width of ~0.5°–3° [*Anderson et al*., 1991]. *Karlsson et al*. [1998] and *He et al*. [2012] found that SAIDs are always located at the equatorial boundary of the auroral particle precipitation and move to lower latitudes with increasing

geomagnetic activities (*Kp*, *Dst*, and *AE*) during substorms. *Spiro et al*. [1979] studied the dependence of SAID occurrence frequency on geomagnetic substorm activities as a function of *AE* index, and *Anderson et al*. [1993] and *Karlsson et al*. [1998] revealed that SAIDs occur mostly during substorms and especially during the substorm recovery phase.

Although SAIDs have been widely studied after their discovery by *Galperin et al*. [1973] and *Spiro et al*. [1979], their solar cycle, seasonal, and diurnal variations, especially solar cycle and diurnal variations, have not been well concerned until now because of the limited coverage of the databases. In this study, we study the solar cycle, seasonal, and diurnal variations of SAID based on the large database from DMSP F8 to F18 satellites during three solar cycles from 1987 to 2012 for the first time.

2. Data Sets and Approach

The DMSP satellites operate in Sun-synchronous orbits at ~800 km altitude with ~99° inclinations and with orbital periods near 100 min. The ion drift meter (IDM), the retarding potential analyzer (RPA), the precipitating energetic particle spectrometer (SSJ/4 and SSJ/5), and the special sensor magnetometer (SSM) on board the DMSP satellites provide the observations of the ion drift velocity [*Greenspan et al*., 1986], ion density [*Greenspan et al*., 1986], the precipitating particle flux [*Hardy et al*., 1984], and the magnetic field [*Rich et al*., 1985], respectively.

According to *Anderson et al*. [1991] and previous studies, SAID events are identified if they fulfill the following criteria: (1) the horizontal WID peak exceeds 1000 m/s, (2) the latitudinal extent is less than 4.0°, (3) the event is located equatorward of auroral zone in dusk to midnight sectors, and (4) the poleward wall of the WID speed curve coincides with or is adjacent to the equatorial boundary of the precipitating electron (EBPE) number fluxes.

In order to study the solar cycle, seasonal, and diurnal variations of these SAID events, the following parameters are considered: (1) UT, the universal time at the WID peak; (2) $SAID_I$, the ILAT of the WID peak; (3) $SAID_T$, the MLT of the WID peak; (4) $SAID_W$, the latitudinal half width of SAID; (5) $EBPE_I$, the ILAT of EBPE; and (6) FAC_I, the ILAT of the peak density (FAC_D) of the downward region 2 field-aligned currents (R2-FAC) calculated with the method in *Anderson et al*. [2001] based on SSM data. Since there are many events with WID peak exceeding the IDM's threshold of 3000 m/s (the true WID peak may achieve ~3500 m/s or greater [e.g., *Puhl-Quinn et al*., 2007]), and the exact peak velocity is difficult to determine, the variations of ion drift velocity are not considered in this study and will be investigated in the future.

Figure 1 illustrates an example of extraction of above parameters. The combination of automatic and manual steps and methods are as follows.

1. Quality checks of the IDM data. Since the RPA and IDM are designed to operate in an O^+ predominant environment, the data quality depends on the light ion concentrations ($[H^+]$ and $[He^+]$). The IDM data are not correct if the light ion concentrations increase over 15% [*Horvath and Lovell*, 2009]. Moreover, if the total plasma density is below 10^3 cm^{-3} or above 10^6 cm^{-3}, the drift data may also be incorrect [*Greenspan et al*., 1986]. For these reasons, each 4 s averaged data point is assigned a quality flag of 1 (reliable), 2 (questionable, use with caution), 3 (poor), or 4 (quality is undetermined) by checking the horizontal drift speed, the light ion percentage, and the total ion density (http://cindispace.utdallas.edu/DMSP/quality.htm) [*Drayton et al*., 2005; *Voiculescu and Roth*, 2008]. For a potential SAID event, if the quality of the data points in the SAID region in Figure 1a is all with flag 1 or 3, this event is automatically accepted or rejected. In addition, if the relative number of points with flag 2, 3, or 4 in the SAID region in Figure 1a is less than 30%, and the spatial variation of the ion drift along the satellite track is smooth, this event can be manually accepted if these points are found to be consistent with the ones with good quality. We manually double check all the accepted and rejected events when the automatic checking procedure is finished. Only events that pass the above filters are judged to be reliable and added to our database.
2. The WID peak is automatically identified from Figure 1a, and the parameters UT, $SAID_I$, and $SAID_T$ are automatically calculated from the orbit data as indicated by the red vertical line in Figure 1a with UT = 05:33:10, $SAID_I = 54.13°$, and $SAID_T = 23.6$ h.
3. The selected region around the WID peak between the two vertical black dotted lines in Figure 1a is fitted using a Voigt function [*Ida et al*., 2000] with Levenberg-Marquardt iteration algorithm to determine $SAID_W$,

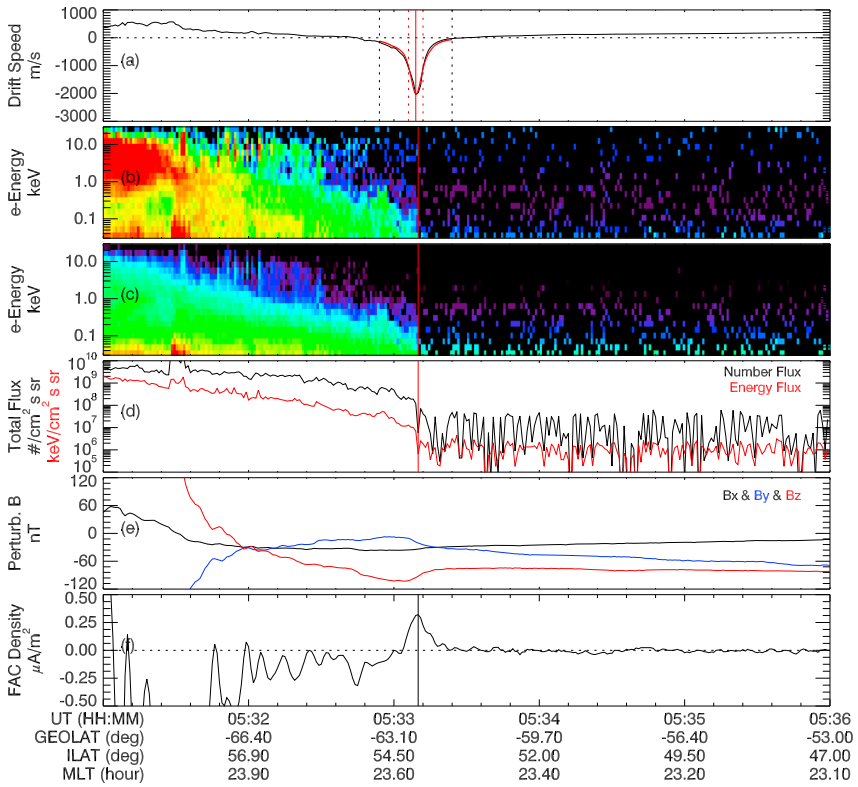

Figure 1. A SAID event observed by DMSP F15 on 20 March 2001. (a) Cross-track drift speed observed by IDM with positive value to be eastward and negative value to be westward. (b) Precipitation electron differential energy flux and (c) differential number flux measured by SSJ/4 between 30 eV and 30 keV. (d) Summarized flux of each energy channel of SSJ/4. (e) Three components of the perturbation magnetic field in the frame of satellite (*z* axis points to the Earth's center, *x* axis is along the fly direction of DMSP, and *y* axis is determined by the right-hand law). (f) FAC density calculated from Figure 1e with positive values representing downward R2-FAC and negative values for upward FAC. Solid vertical lines represent the WID peak in Figure 1a, EBPE in Figures 1b and 1c, and peak R2-FAC density in Figure 1f, respectively. The black dashed vertical lines in Figure 1a confine the fitting area for drift speed, and the red dashed vertical lines illustrate fitted FWHM.

which can be denoted by the full width at half maximum (FWHM) of the Voigt function. The fitted speed is overlapped in Figure 1a with red color, and $SAID_W = 0.25°$ is confined by the two vertical red dotted lines.

4. Determination of $EBPE_I$. Figures 1b and 1c show the precipitation electron energy flux and number flux simultaneously measured by SSJ, respectively. The determination of EBPE is similar to that of plasmapause in EUV images [*Sandel et al.*, 2003]; that is, the location where the total energy flux (red) and total number flux (black) in Figure 1d drops abruptly is identified as boundary. The energy flux is preferred in this process, and the number flux is considered if the energy flux is not available. The extracted EBPE ($EBPE_I = 54.08°$) is marked by vertical lines in Figures 1b–1d.
5. Figure 1e displays the three components of the perturbed magnetic field. Since at the altitude of the DMSP satellite (~800 km), the magnetometer is only sensitive to the magnetospheric FAC, and the contribution of ionospheric currents can thus be neglected. FAC is assumed to be infinite sheets aligned with auroral oval, also known as L shell alignment. The two assumptions are reliable and have been adopted in previous works [*Higuchi and Ohtani*, 2000; *Figueiredo et al.*, 2004]. It is noted that on F12–F14, the SSM instrument was mounted on the body of the spacecraft. This led to significant periodic noise. The SSM data used in this study were retrieved directly from National Geophysical Data Center (NGDC), and the noise was not removed. In order to use these data, a fast Fourier transform filter is used to smooth out the noise. According to Ampere-Maxwell's law and applying the discrete magnetic field samples [*Lühr et al.*, 1996], FAC_D is $1/\mu_0 \times \Delta B/(v_h \Delta t)$, where ΔB is the projection of the perturbation horizontal magnetic field (*y* and *z* components) on the current sheet tangential direction measured by SSM, v_h is the projection of the horizontal velocity component of the spacecraft on the current sheet normal direction, and Δt is the sampling time of the magnetic fields (time constant 1 s for SSM). Once the FAC_D are estimated along a

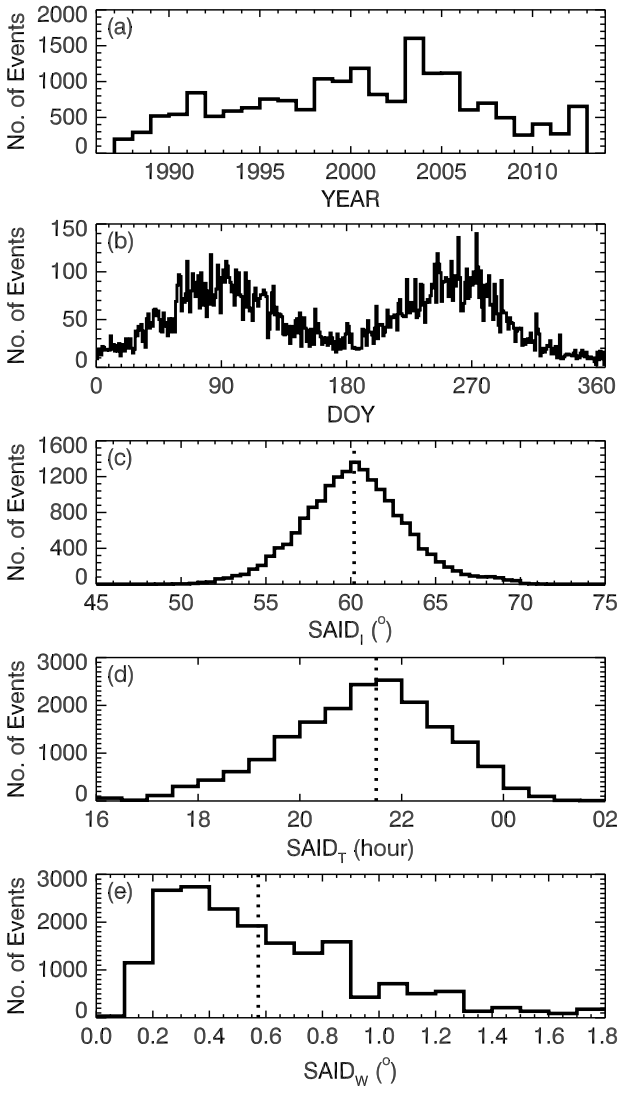

Figure 2. Number of SAID events as a function of (a) year (binned in 1 year intervals), (b) day of year (DOY, binned in 1 day intervals), (c) ILAT of SAID (SAID$_I$, binned in 0.5° intervals), (d) MLT of SAID (SAID$_T$, binned in 0.5 h intervals), and (e) half width of SAID (SAID$_W$, binned in 0.1° intervals). The vertical dashed lines in Figures 2c–2e represent the statistical means.

DMSP orbit, FAC$_I$ can also be extracted. The calculated FAC density is shown in Figure 1f with FAC$_I$ = 54.07° and FAC$_D$ = 0.32 μA/m^2, as marked by the vertical line. It is noted that the SSM data from DMSP F12 through F18 after 1995 are used for the FAC calculations since F8 through F11 did not have a SSM on board and no magnetic field data are available before 1995 from NGDC.

Using above methods, a database was compiled consisting of 18,226 SAID events identified from DMSP F8 to F18 during 1987–2012, in which 72.1% were identified using all the IDM, SSJ, and SSM data, 23.6% were identified using only the IDM and SSJ data, and the remaining 4.3% were identified using only the IDM data. Figure 2 shows the basic information of the database versus year, day of year (DOY), SAID$_T$, SAID$_I$, and SAID$_W$, respectively. Figure 2a reveals that SAID events are not uniformly encountered in each year. The number of satellites in orbits and data availability might result in such yearly distribution of SAID occurrence.

The most significant result in Figure 2b is that two peaks occur at the time of spring and fall equinoxes and two valleys occur at the time of summer and winter solstices. The semiannual variation of SAID occurrence is in consistent with the results of *Karlsson et al.* [1998] using Freja data and *He et al.* [2012] using DE-2, Akebono, and Astrid-2 data. The SAID events occur mostly at 60.1° ILAT and 2130 MLT as shown by the vertical dashed lines in Figures 2c and 2d with a majority between 56° and 65° and between 2000 and 2300 MLT, respectively, in agreement with previous statistical studies [*Karlsson et al.*, 1998; *Figueiredo et al.*, 2004]. SAID$_W$ in Figure 2e is between 0.05° and 1.8° with a mean value of 0.57°, which is also in consistent with the value of 0.05°–1.4° in *Karlsson et al.* [1998].

Regarding the distributions in Figures 2a, 2b, and 2d, the distribution patterns may have resulted from the idiosyncrasies of the DMSP orbits which are MLT or local time bounded. So it is better to do the analysis using the normalized occurrence frequency instead of number of events. The number of satellite orbits and the normalized occurrence frequencies are shown in Figures 3 and 4. Figure 3a shows the number of satellite orbits as a function of year, and the corresponding occurrence frequency of SAID events are displayed in Figure 3c, dashed lines in both panels represent the scaled yearly averaged sunspot number. There seems to be no obvious correlation between the occurrence frequency and the sunspot number. Figures 3b and 3d present the number of satellite orbits and the occurrence frequency of SAID events as a function of DOY, respectively. The number of satellite orbits changes little with DOY; thus, the distribution of SAID occurrence

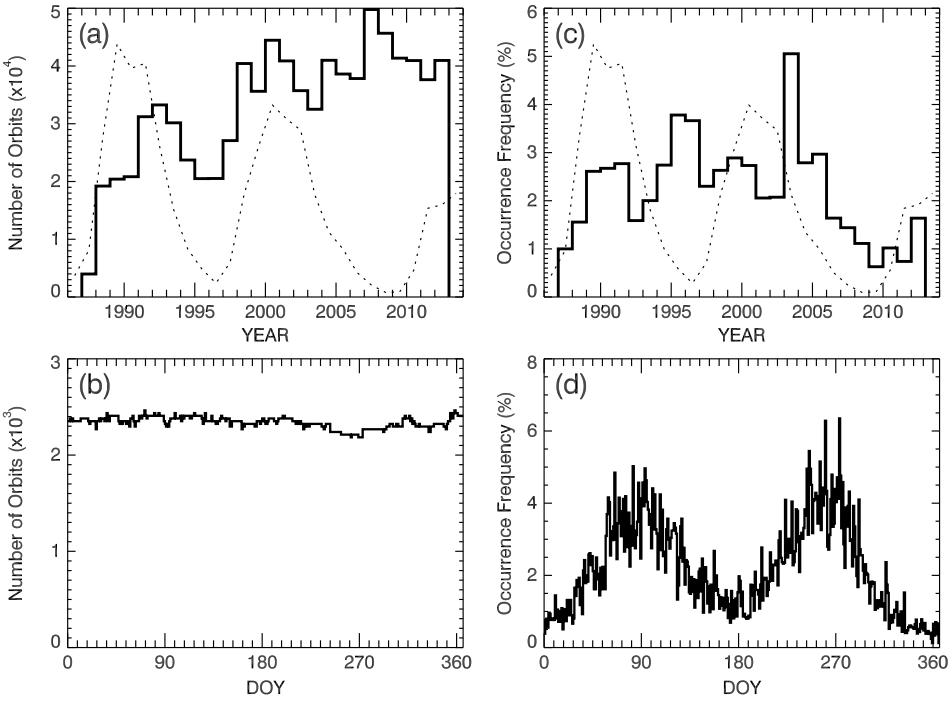

Figure 3. Number of DMSP F8–F18 satellite orbits as a function of (a) year (binned in 1 year intervals) and (b) day of year (DOY, binned in 1 day intervals). The occurrence frequencies of SAID as a function of (c) year (binned in 1 year intervals) and (d) DOY, binned in 1 day intervals. The dashed lines in Figures 3a and 3c represent the yearly averaged sunspot number normalized to the range of *y* axis.

frequency versus DOY is similar to Figure 2b, revealing that SAID events do happen more frequently in spring and fall than in summer and winter.

In order to better describe the ILAT and MLT distributions of the SAID occurrence, a set of bins divided by the MLT (half hour bins) between 16 and 2 h and the ILAT (2.5° bins) between 50° and 70° is created. All the orbital passes from DMSP F8 through F18 are sampled to get the two-dimensional (2-D) orbital passes distribution in Figure 4a by checking each orbital pass and counting each and all the bins that pass goes through. A similar process would be done to create a 2-D distribution in these bins for all the SAID events as shown in Figure 4b. Then the SAID events distribution is normalized against the orbital passes distribution to get the 2-D SAID occurrences distribution in Figure 4c. It is noted that most of the orbital passes are in the dawn sector in Figure 4a and most of the SAID events happen at 60.0° ILAT and 2130 MLT as indicated by the white cross in Figure 4b with the same mean values as in Figures 2c and 2d, respectively. However, Figure 4c indicates that the

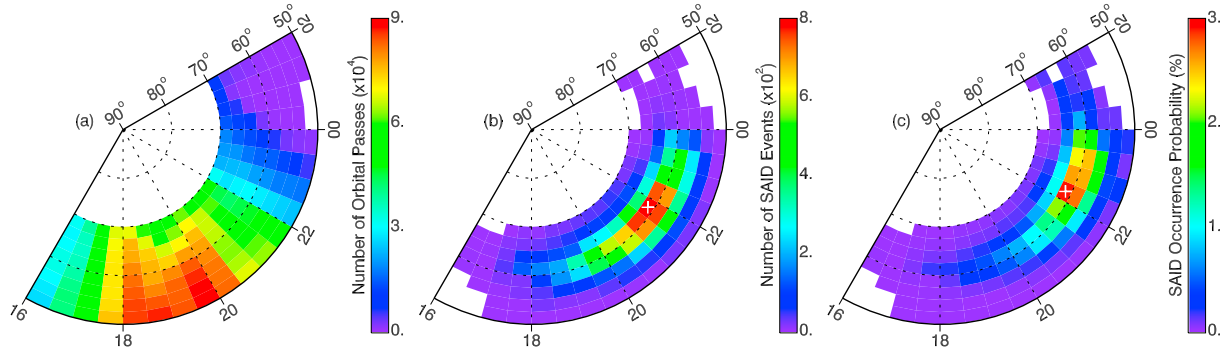

Figure 4. Polar contour of (a) the orbital passes distribution for DMSP F8–F18, (b) the SAID events distribution, and (c) the normalized SAID occurrence probability distribution in MLT (binned in 0.5 h intervals between 16 and 2 h) with midnight at right and ILAT (binned in 2.5° intervals between 50° and 70°). The maximums in Figures 4b and 4c are marked by the white crosses, respectively.

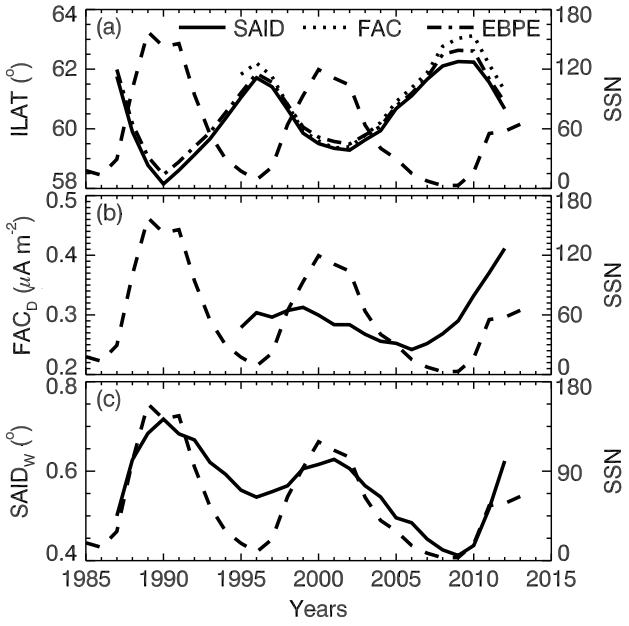

Figure 5. Solar cycle variations of SAID. Shown are the yearly averaged (a) $SAID_I$ (solid line), FAC_I (dotted line), and $EBPE_I$ (dash-dotted line), (b) FAC_D, and (c) $SAID_W$. Dashed lines in Figures 5a–5c represent the SSN with axes displayed at right.

maximum probability of SAID occurrence is found at the same ILAT with Figure 4b but at 2230 MLT in the premidnight sector as marked by the white cross, and the low occurrence probabilities show that SAID events are quite rare before 1800 MLT and after 0100 MLT.

3. Statistical Results and Discussions

The large number of SAID events during 26 years is a good basis for investigating the statistical properties of SAID. The solar cycle, seasonal, and diurnal variations of SAID have been investigated in the following sections.

3.1. Solar Cycle Variations

Figure 5 presents solar cycle variations of the yearly averaged $SAID_I$, $EBPE_I$, FAC_I, FAC_D, and $SAID_W$, and Table 1 lists the nonparametric Spearman rank-order correlation coefficients r^S and their corresponding significance levels p [*Press et al.*, 1992] between these parameters and the solar activity represented by the yearly averaged sunspot number (SSN) throughout the three cycles (22, 23, and 24). The most important result in Figure 5 is that SAIDs are strongly correlated to solar activities for such a long time coverage, which is found for the first time. $SAID_I$, $EBPE_I$, and FAC_I in Figure 5a are significantly negatively correlated to solar activity with r^S equal or below -0.9 and $p < 10^{-4}$, and $SAID_W$ in Figure 5c is significantly positively correlated to solar activity with $r^S > 0.9$ and $p < 10^{-4}$. Correlation of FAC_D to solar activity in Figure 5b is less significant than other parameters. The correlation of $SAID_I$ to solar activity is in consistent with the correlation of SAPS to geomagnetic activity [*Foster and Vo*, 2002]. This is very natural since the geomagnetic activity is positively correlated to solar activity.

SAIDs associated with substorms are the prominent phenomena of the coupled MI system which are controlled by the solar activities. $SAID_I$ is controlled by the boundary latitudes of aurora and electron precipitation during substorms, the strengths of which are proportional to the solar activities [*Nevanlinna and Pulkkinen*, 1998]. The significant results in Figure 5a indicate that SAIDs occur more equatorward during high solar activities and more poleward during low solar activities. The strongly positive correlation of $SAID_W$ to solar activities as shown in Table 1 may be resulted from the fact that the strength of partial ring current increases and its domain increases during high solar activities. These results may illustrate that the region of SAID coincides with the part of R2-FAC which is downward of the partial ring current and located equatorward of EBPE, a theory that is consistent with the conclusions from *Anderson et al.* [1993] and *Karlsson et al.* [1998].

Table 1. Correlation Coefficients r^S and Their Corresponding Significance Levels p Between SAID and SSN From Cycle 22 to Cycle 24

	Cycle 22		Cycle 23		Cycle 24		All Cycles	
	r^S	p	r^S	p	r^S	p	r^S	p
$SAID_I$	−0.93	0.0008	−0.91	$<10^{-4}$	−0.88	$<10^{-4}$	−0.90	$<10^{-4}$
$EBPE_I$	−0.89	0.0007	−0.91	$<10^{-4}$	−0.92	$<10^{-4}$	−0.91	$<10^{-4}$
FAC_I	N/A[a]	N/A[a]	−0.88	$<10^{-4}$	−0.91	$<10^{-4}$	−0.90	$<10^{-4}$
$SAID_W$	0.96	0.0002	0.94	$<10^{-4}$	0.83	$<10^{-4}$	0.92	$<10^{-4}$
FAC_D	N/A[a]	N/A[a]	0.46	0.1120	0.96	0.0001	0.56	0.1007

[a]The DMSP SSM data are available only from 1995 in cycle 23.

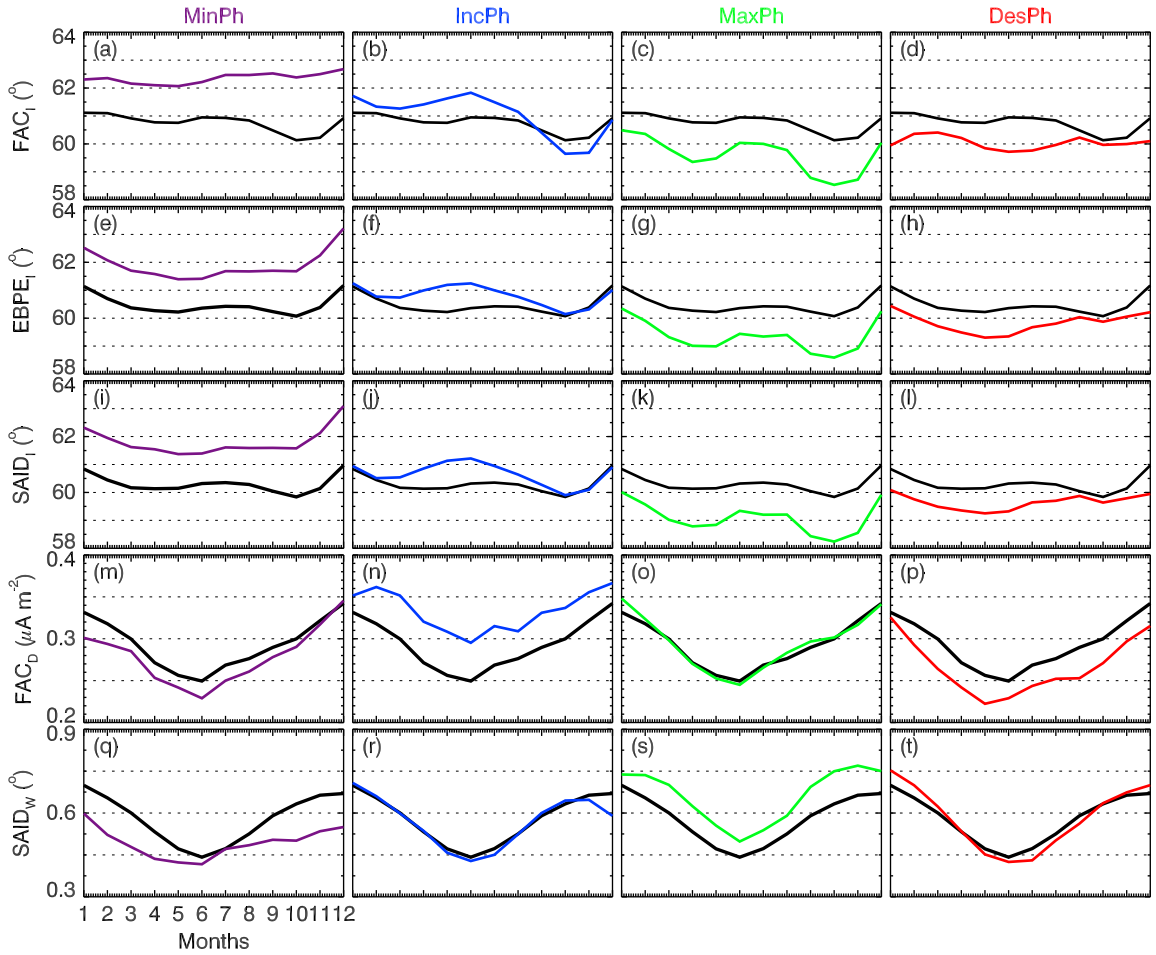

Figure 6. Seasonal variations of SAID and FAC. Shown are the monthly averaged (a–d) FAC_I, (e–h) $EBPE_I$, (i–l) $SAID_I$, (m–p) FAC_D, and (q–t) $SAID_W$. Black thick lines represent the monthly averaged values for all solar cycle phases. Colored lines correspond to variations in different solar cycle phases as indicated at the top.

3.2. Seasonal Variations

The seasonal variations of $SAID_I$, $EBPE_I$, FAC_I, FAC_D, and $SAID_W$ are shown in Figure 6. Each column in Figure 6 represents a solar cycle phase as indicated at the top, and the averages for all the solar cycle phases are also shown by the black lines in each panel. A solar cycle is divided into four phases, namely, minimum phase (MinPh), increasing phase (IncPh), maximum phase (MaxPh), and descending phase (DesPh) according to the method proposed in *Ouattara et al.* [2009].

The seasonal variations of $SAID_I$, $EBPE_I$, and FAC_I are similar and are characterized by spring and fall valleys in Figures 6a–6l which are in consistent with *Wang et al.* [2008]. Their similarity in seasonal variation and the significant correlations shown in Table 2 indicate that the generation mechanism of SAID associated with the electron precipitation and the downward FAC is in agreement with that proposed by *Anderson et al.* [1993]. This seasonal variation seems to result from the Russell-McPherron effect [*Russell and McPherron*, 1973]. According to Russell-McPherron effect, the geomagnetic activity is strong during spring and fall while weak during summer and winter. As the geomagnetic activity becomes strong, the equatorial boundary of auroral oval moves to low latitude, causing the decrease of $SAID_I$, $EBPE_I$, and FAC_I. According to *Russell and Mcpherron* [1973], the spring peak of

Table 2. Cross Correlations of $SAID_I$ to $EBPE_I$ and FAC_I, and $SAID_W$ to FAC_D

	Seasonal		Diurnal	
	r^S	p	r^S	p
$SAID_I$-$EBPE_I$	0.97	$<10^{-4}$	0.96	$<10^{-4}$
$SAID_I$-FAC_I	0.81	0.0022	0.81	$<10^{-4}$
$SAID_W$-FAC_D	0.96	$<10^{-4}$	0.98	$<10^{-4}$

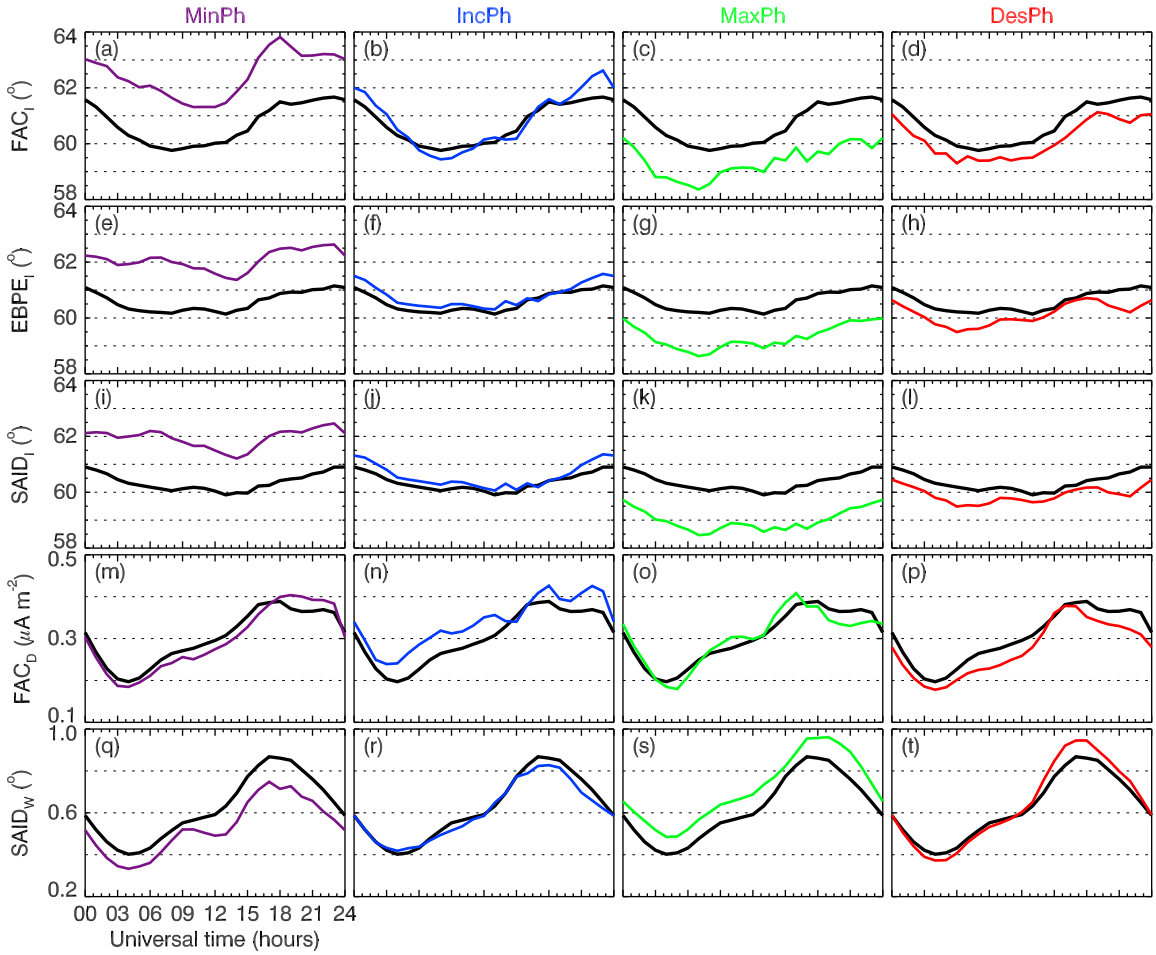

Figure 7. Diurnal variations of SAID. The format is the same as Figure 6.

geomagnetic activity is weaker than the fall peak, so the valleys are somewhat weak in spring in Figures 6a–6l. Meanwhile, the Russell-Mcpherron effect is more apparent during active years (see Figure 1 in *Russell and McPherron* [1973]) so that the seasonal variations are the most significant in MaxPh as shown in Figures 6c, 6g, and 6k.

The significant seasonal variations of $SAID_W$ and FAC_D in Figures 6m–6t exhibit clear "V" signatures with the minimums occurring in summer (0.4° and 0.25 $\mu A\,cm^{-2}$) and the maximums occurring in winter (~0.8° and 0.35 $\mu A\,cm^{-2}$), respectively. The seasonal variations of FAC_D are in agreement with the simulation results of *Hurtaud et al.* [2007]. The high correlation between $SAID_W$ and FAC_D in Table 2 illustrates that the seasonal variations of $SAID_W$ may be mainly controlled by seasonal variations of the strength of downward FAC. Phase-to-phase variations are also obvious for all the parameters and are somewhat in agreement with the solar cycle variations in Figure 5. However, the seasonal variations in different solar cycle phases show some differences as indicated by the colored lines in Figure 6. The valleys of $SAID_I$, $EBPE_I$, and FAC_I occur in different seasons in different phases. The amplitudes of the phase-to-phase variations are larger after September for $SAID_I$, $EBPE_I$, and FAC_I than before September, and the amplitude for $SAID_W$ decreases from the beginning of the year to June and then increases continuously to the end of the year.

3.3. Diurnal Variations

Figure 7 presents the diurnal variations of $SAID_I$, $EBPE_I$, FAC_I, FAC_D, and $SAID_W$ for different solar cycle phases. The diurnal variations of $SAID_I$, $EBPE_I$, and FAC_I are simple in Figures 7a–7l: lower by day with values of ~60.0° and higher at night with values of 61.0°, 61.0°, and 62.0°, respectively. However, the day-to-night difference

of FAC_I is larger (~2.0°) than those of $SAID_I$ and $EBPE_I$ (~1.0°). The similarity (or high correlations) in diurnal variations of $SAID_I$, $EBPE_I$, and FAC_I in Table 2 also supports the SAID generation mechanism mentioned in section 3.2. The significant diurnal variations of both $SAID_W$ and FAC_D in Figures 7m–7t are similar to inverted sine curves. The minimums occur at 0400 UT (0.4° and 0.2 $\mu A\,cm^{-2}$), and the maximums occur at 1700 UT (0.9° and 0.4 $\mu A\,cm^{-2}$). The high correlation between $SAID_W$ and FAC_D in Table 2 indicates that the diurnal variations of $SAID_W$ may be mainly controlled by diurnal variations of the strength of downward FAC.

The diurnal variations of $SAID_I$, $EBPE_I$, FAC_I, FAC_D, and $SAID_W$ for different solar cycle phases show similar variation patterns as indicated by the colored lines in Figure 7. The diurnal variations of $SAID_I$, $EBPE_I$, and FAC_I under different solar cycle phases are similar to the all-phase-averaged variations, respectively. It is noted that $SAID_I$, $EBPE_I$, and FAC_I move poleward for MinPh and equatorward for MaxPh, and approach the averages for IncPh and DesPh, but are more poleward for IncPh, respectively.

The clear diurnal variations of FAC_I, $SAID_W$, and FAC_D might be explained as follows. According to *Deminov and Shubin* [1987], *Anderson et al*. [1993], and *De Keyser et al*. [1998], R2-FAC is an important driven factor of a SAID event. It is known that the R2-FAC is closely related to variations of the partial ring current as well as the geomagnetic disturbances [*Tsyganenko*, 2000]. The diurnal variations of the partial ring current [*O'Brien and McPherron*, 2002] and the geomagnetic disturbances [*Russell*, 1989; *Cliver et al*., 2000] might cause such diurnal variation of R2-FAC. As to the diurnal variation of $SAID_W$, it may be controlled by the strength of R2-FAC since the width of the WID region reflects the energy input from R2-FAC. More energy input results in stronger frictional heating of subauroral ionospheric ions as well as greater reduction of the height-integrated Pedersen conductivity [*Anderson et al*., 1993], and a latitudinally wider WID region is generated thereafter. Above discussion is just a possible explanation of the diurnal variations of SAID and R2-FAC, and the mechanism to produce such diurnal variations and their correlations with cross polar cap potential, Pedersen conductivity, and ion temperature can be further studied in the future.

4. Summary and Conclusion

The large database of 18,226 SAID events observed by DMSP satellites for three solar cycles (1987–2012) is used for the first time to study the solar cycle, seasonal, and diurnal variations of SAID. Statistical results show that SAIDs occur mostly at 60.1° ILAT and 2230 MLT with majority between 56° and 65° and between 2000 and 2300 MLT, respectively, which is in consistent with previous statistical studies [*Karlsson et al*., 1998; *Figueiredo et al*., 2004]; the half widths of SAID are between 0.05° and 1.8° with a mean value of 0.57° in agreement with the value of 0.05°–1.4° in *Karlsson et al*. [1998], and the occurrences of SAID have two peaks in spring and fall equinoxes and two valleys in summer and winter solstices, also in consistent with the result of *Karlsson et al*. [1998].

The most important findings are that SAID events have clear solar cycle, seasonal, and diurnal variations for four solar cycle phases. SAIDs occur more equatorward during high solar activities with larger latitudinal widths and more poleward during low solar activities with smaller latitudinal widths. The seasonal variations of the ILATs of SAID, EBPE, and R2-FAC have two valleys in spring and fall, in consistent with *Wang et al*. [2008]. The half widths of SAID and the density of R2-FAC decrease from the beginning of a year until June and then increase continuously to the end of the year. The diurnal variations of SAID, EBPE, and R2-FAC exhibit a clear day-to-night difference in ILAT. The significant diurnal variations of both $SAID_W$ and FAC_D are similar to inverted sine curves with minimums at 0400 UT and maximums at 1700 UT, respectively.

The high correlations of $SAID_I$ to both $EBPE_I$ and FAC_I indicate that the generation mechanism of SAID associated with the electron precipitation and the downward FAC is in agreement with that proposed by *Anderson et al*. [1993]. The high correlation between FAC_D and $SAID_W$ indicates that the $SAID_W$ may be mainly controlled by the strength of downward FAC. This might support that SAIDs are the production of magnetosphere-ionosphere coupling, and the generation of SAID may be mainly controlled by the electron precipitation and the FAC during substorms. According to both this study and past works [e.g., *Foster and Vo*, 2002], SAID is highly correlated to solar and geomagnetic activities, and the latter is basically driven by the solar wind and interplanetary magnetic field (SW-IMF) conditions. In future work, we will systematically investigate the relationship between SAID parameters and SW-IMF conditions.

Acknowledgments
The authors sincerely thank NOAA/NESDIS/National Geophysical Data Center for the provision of the DMSP IDM, SSJ/4, and SSM data. The sunspot number is provided by SPIDR at NGDC. This work was supported by the National Basic Research Program of China (2012CB957800 and 2011CB811400), the National Natural Science Foundation of China (41204102 and 41274147), and the National Hi-Tech Research and Development Program of China (2012AA121000).

Yuming Wang thanks Pamela Puhl-Quinn and an anonymous reviewer for their assistance in evaluating this paper.

References

Anderson, P. C. (2004), Subauroral electric fields and magnetospheric convection during the April, 2002 geomagnetic storms, *Geophys. Res. Lett.*, *31*, L11801, doi:10.1029/2004GL019588.

Anderson, P. C., R. A. Heelis, and W. B. Hanson (1991), The ionosphere signatures of rapid subauroral ion drifts, *J. Geophys. Res.*, *96*(A4), 5785–5792, doi:10.1029/90JA02651.

Anderson, P. C., W. B. Hanson, R. A. Heelis, J. D. Craven, D. N. Baker, and L. A. Frank (1993), A proposed production model of rapid subauroral ion drifts and their relationship to substorm evolution, *J. Geophys. Res.*, *98*(A4), 6069–6078, doi:10.1029/92JA01975.

Anderson, P. C., D. L. Carpenter, K. Tsuruda, T. Mukai, and F. J. Rich (2001), Multisatellite observations of rapid subauroral ion drifts (SAID), *J. Geophys. Res.*, *106*(A12), 29,585–29,599, doi:10.1029/2001JA000128.

Cliver, E. W., Y. Kamide, and A. G. Ling (2000), Mountains and valleys: Semiannual variation of geomagnetic activity, *J. Geophys. Res.*, *105*(A2), 2413–2424, doi:10.1029/1999JA900439.

De Keyser, J., M. Roth, and J. Lemaire (1998), The magnetospheric driver of subauroral ion drifts, *Geophys. Res. Lett.*, *25*(10), 1625–1628, doi:10.1029/98GL01135.

Deminov, M. G., and V. N. Shubin (1987), Dynamics of the subauroral ionosphere under disturbance conditions, *Geomagn. Aeron., Engl. Transl.*, *27*, 398.

Drayton, R. A., A. V. Koustov, M. R. Hairston, and J.-P. Villain (2005), Comparison of DMSP cross-track ion drifts and SuperDARN line-of-sight velocities, *Ann. Geophys.*, *23*, 2479–2486, doi:10.5194/angeo-23-2479-2005.

Figueiredo, S., T. Karlsson, and G. T. Marklund (2004), Investigation of subauroral ion drifts and related field-aligned currents and ionospheric Pedersen conductivity distribution, *Ann. Geophys.*, *22*, 923–934.

Foster, J. C., and H. B. Vo (2002), Average characteristics and activity dependence of the subauroral polarization stream, *J. Geophys. Res.*, *107*(A12), 1475, doi:10.1029/2002JA009409.

Foster, J. C., and W. J. Burke (2002), SAPS: A new categorization for sub-auroral electric fields, *Eos. Trans. AGU*, *83*(36), 393–394, doi:10.1029/2002EO000289.

Foster, J. C., M. J. Buonsanto, M. Mendillo, D. Nottingham, F. J. Rich, and W. Denig (1994), Coordinated stable auroral red arc observations: Relationship to plasma convection, *J. Geophys. Res.*, *99*(A6), 11,429–11,439, doi:10.1029/93JA03140.

Foster, J. C., P. J. Erickson, F. D. Lind, and W. Rideout (2004), Millstone Hill coherent-scatter radar observations of electric field variability in the sub-auroral polarization stream, *Geophys. Res. Lett.*, *31*, L21803, doi:10.1029/2004GL021271.

Galperin, Y. I., Y. N. Ponomarov, and A. G. Zosinova (1973), Direct measurements of ion drift velocity in the upper ionosphere during a magnetic storm, *Cosmicheskie Issled.*, *11*, 273.

Goldstein, J., J. L. Burch, and B. R. Sandel (2005), Magnetospheric model of subauroral polarization stream, *J. Geophys. Res.*, *110*, A09222, doi:10.1029/2005JA011135.

Greenspan, M. E., P. B. Anderson, and J. M. Pelagatti (1986), Characteristics of the thermal plasma monitor (SSIES) for the defense meteorological satellite program (DMSP) spacecraft S8 through S10, Tech. Rep. AFGL-TR-86-0227, Air Force Geophys. Lab., Hanscom Air Force Base, Mass.

Hardy, D. A., H. C. Yeh, L. K. Schmitt, T. L. Schumaker, M. S. Gussenhoven, A. Huber, F. J. Marshall, and J. Pantazis (1984), Precipitating electron and ion detectors (SSJ/4) on the block 5D/Flights 6-10 DMSP satellites: Calibration and data presentation, Tech. Rep. AFGL-TR-84-0317, Air Force Geophys. Lab., Hanscom Air Force Base, Mass.

He, F., X. X. Zhang, B. Chen, and M.-C. Fok (2012), Plasmaspheric trough evolution under different conditions of subauroral ion drift, *Sci. China. Tech. Sci.*, *55*(5), 1–8, doi:10.1007/s11431-012-4781-1.

Higuchi, T., and S.-I. Ohtani (2000), Automatic identification of large-scale field-aligned current structures, *J. Geophys. Res.*, *105*(A11), 25,305–25,315, doi:10.1029/2000JA900073.

Horvath, I., and B. C. Lovell (2009), Investigating the relationships among the South Atlantic Magnetic Anomaly, southern nighttime midlatitude trough, and nighttime Weddell Sea Anomaly during southern summer, *J. Geophys. Res.*, *114*, A02306, doi:10.1029/2008JA013719.

Huang, C.-S., and J. C. Foster (2007), Correlation of the subauroral polarization streams (SAPS) with the Dst index during severe magnetic storms, *J. Geophys. Res.*, *112*, A11302, doi:10.1029/2007JA012584.

Hurtaud, Y., C. Peymirat, and A. D. Richmond (2007), Modeling seasonal and diurnal effects on ionospheric conductances, region-2 currents, and plasma convection in the inner magnetosphere, *J. Geophys. Res.*, *112*, A09217, doi:10.1029/2007JA012257.

Ida, T., M. Ando, and H. Toraya (2000), Extended pseudo-Voigt function for approximating the Voigt profile, *J. Appl. Cryst.*, *33*, 1311–1316.

Karlsson, T., G. T. Marklund, and L. G. Blomberg (1998), Subauroral electric fields observed by the Freja satellite: A statistical study, *J. Geophys. Res.*, *103*(A3), 4327–4314, doi:10.1029/97JA00333.

Lühr, H., J. Warnecke, and M. K. A. Rother (1996), An algorithm for estimating field-aligned currents from single spacecraft magnetic field measurements: A diagnostic tool applied to Freja satellite data, *Geosci. Remote Sens.*, *34*, 1369–1376.

Lyatsky, W., A. Tan, and G. V. Khazanov (2006), A simple analytical model for subauroral polarization stream (SAPS), *Geophys. Res. Lett.*, *33*, L19101, doi:10.1029/2006GL025949.

Maynard, N. C., T. L. Aggson, and J. P. Heppner (1980), Magnetospheric observation of large subauroral electric fields, *Geophys. Res. Lett.*, *7*(11), 881–884, doi:10.1029/GL007i011p00881.

Mishin, E. V., and P. A. Puhl-Quinn (2007), SAID: Plasmaspheric short circuit of substorm injections, *Geophys. Res. Lett.*, *34*, L24101, doi:10.1029/2007GL031925.

Nevanlinna, H., and T. I. Pulkkinen (1998), Solar cycle correlations of substorm and auroral occurrence frequency, *Geophys. Res. Lett.*, *25*(16), 3087–3090, doi:10.1029/98GL02335.

O'Brien, T. P., and R. L. McPherron (2002), Seasonal and diurnal variation of Dst dynamics, *J. Geophys. Res.*, *107*(A11), 1341, doi:10.1029/2002JA009435.

Ober, D. M., J. L. Horwitz, and D. L. Gallagher (1997), Formation of density troughs embedded in the outer plasmasphere by subauroral ion drift events, *J. Geophys. Res.*, *102*(A7), 14,595–14,602, doi:10.1029/97JA01046.

Oksavik, K., R. A. Greenwald, J. M. Ruohoniemi, M. R. Hairston, L. J. Paxton, J. B. H. Baker, J. W. Gjerloev, and R. J. Barnes (2006), First observations of the temporal/spatial variation of the sub-auroral polarization stream from the SuperDARN Wallops HF radar, *Geophys. Res. Lett.*, *33*, L12104, doi:10.1029/2006GL026256.

Ouattara, F., C. Amory-Mazaudier, R. Fleury, P. Lassudrie Duchesne, P. Vila, and M. Petitdidier (2009), West African equatorial ionospheric parameters climatology based on Ouagadougou ionosonde station data from June 1966 to February 1998, *Ann. Geophys.*, *27*, 2503–2514.

Pintér, B., S. D. Thom, R. Balthazor, H. Vo, and G. J. Bailey (2006), Modeling subauroral polarization streams equatorward of the plasmapause footprints, *J. Geophys. Res.*, *111*, A10306, doi:10.1029/2005JA011457.

Press, W. H., S. A. Teukolsky, W. T. Vetterling, and B. P. Flannery (1992), *Numerical Recipes*, Cambridge Univ. Press, Cambridge, U. K.
Puhl-Quinn, P. A., H. Matsui, E. Mishin, C. Mouikis, L. Kistler, Y. Khotyaintsev, P. M. E. Décréau, and E. Lucek (2007), Cluster and DMSP observations of SAID electric fields, *J. Geophys. Res.*, *112*, A05219, doi:10.1029/2006JA012065.
Rich, F. J., W. J. Burke, M. C. Kelley, and M. Smiddy (1980), Observations of FAC in association with strong convection electric fields at subauroral latitudes, *J. Geophys. Res.*, *85*(A5), 2335–2340, doi:10.1029/JA085iA05p02335.
Rich, F. J., D. A. Hardy, and M. S. Gussenhoven (1985), Enhanced ionosphere magnetosphere data from the DMSP satellites, *Eos. Trans. AGU*, *66*(26), 513–514, doi:10.1029/EO066i026p00513.
Russell, C. T. (1989), The universal time variation of geomagnetic activity, *Geophys. Res. Lett.*, *16*(6), 555–558, doi:10.1029/GL016i006p00555.
Russell, C. T., and R. L. McPherron (1973), Semiannual variation of geomagnetic activity, *J. Geophys. Res.*, *78*(1), 92–108, doi:10.1029/JA078i001p00092.
Sandel, B. R., J. Goldstein, D. L. Gallagher, and M. Spasojević (2003), Extreme ultraviolet imager observations of the structure and dynamics of the plasmasphere, *Space Sci. Rev.*, *109*(1), 25–46.
Spiro, R. W., R. A. Heelis, and W. B. Hanson (1978), Ion convection and the formation of the midlatitude F region ionization trough, *J. Geophys. Res.*, *83*(A9), 4255–4264, doi:10.1029/JA083iA09p04255.
Spiro, R. W., R. H. Heelis, and W. B. Hanson (1979), Rapid subauroral ion drifts observed by Atmospheric Explorer C, *Geophys. Res. Lett.*, *6*(8), 657–660, doi:10.1029/GL006i008p00657.
Tsyganenko, N. A. (2000), Modeling the inner magnetosphere: The asymmetric ring current and Region 2 Birkeland currents revisited, *J. Geophys. Res.*, *105*(A2), 27,739–27,754, doi:10.1029/2000JA000138.
Voiculescu, M., and M. Roth (2008), Eastward sub-auroral ion drifts or ASAID, *Ann. Geophys.*, *26*, 1955–1963, doi:10.5194/angeo-26-1955-2008.
Wang, H., A. J. Ridley, H. Lühr, M. W. Liemohn, and S. Y. Ma (2008), Statistical study of the subauroral polarization stream: Its dependence on the cross-polar cap potential and subauroral conductance, *J. Geophys. Res.*, *113*, A12311, doi:10.1029/2008JA013529.
Wang, H., H. Lühr, and S. Y. Ma (2012), The relation between subauroral polarization streams, westward ion fluxes, and zonal wind: Seasonal and hemispheric variations, *J. Geophys. Res.*, *117*, A04323, doi:10.1029/2011JA017378.
Yeh, H.-C., J. C. Foster, F. J. Rich, and W. Swider (1991), Storm time electric field penetration observed at mid-latitude, *J. Geophys. Res.*, *96*(A4), 5707–5721, doi:10.1029/90JA02751.
Zheng, Y., P. C. Brandt, A. T. Y. Lui, and M.-C. Fok (2008), On ionospheric trough conductance and subauroral polarization streams: Simulation results, *J. Geophys. Res.*, *113*, A04209, doi:10.1029/2007JA012532.